Hot Hydride Superconductivity Above 550 K

A. D. Grockowiak[1,2]*, M. Ahart[3], T. Helm[4,5], W. A. Coniglio[1], R. Kumar[3], K. Glazyrin[6], G. Garbarino[7], Y. Meng[8], M. Oliff[1], V. Williams[1], N. W. Ashcroft[9], R. J. Hemley[3,10], M. Somayazulu[8] and S. W. Tozer[1]*

[1]National High Magnetic Field Laboratory, Florida State University, Tallahassee, FL, United States, [2]Brazilian Synchrotron Light Laboratory (LNLS/Sirius), Brazilian Center for Research in Energy and Materials (CNPEM), Campinas, Brazil, [3]Department of Physics, University of Illinois Chicago, Chicago, IL, United States, [4]Dresden High Magnetic Field Laboratory (HLD-EMFL), Helmholtz-Zentrum Dresden-Rossendorf, Dresden, Germany, [5]Max Planck Institute for Chemical Physics of Solids, Dresden, Germany, [6]DESY (Deutsches Elektronen Synchrotron), Hamburg, Germany, [7]European Synchrotron Radiation Facility (ESRF), Grenoble, France, [8]HPCAT, X-ray Science Division, Argonne National Laboratory, Lemont, IL, United States, [9]Laboratory of Atomic and Solid State Physics, Cornell University, Ithaca, NY, United States, [10]Department of Chemistry, University of Illinois Chicago, Chicago, IL, United States

The search for room temperature superconductivity has accelerated in the last few years driven by experimentally accessible theoretical predictions that indicated alloying dense hydrogen with other elements could produce conventional superconductivity at high temperatures and pressures. These predictions helped inform the synthesis of simple binary hydrides that culminated in the discovery of the superhydride LaH_{10} with a superconducting transition temperature T_c of 260 K at 180 GPa. We have now successfully synthesized a metallic La-based superhydride with an initial T_c of 294 K. When subjected to subsequent thermal excursions that promoted a chemical reaction to a higher order system, the T_c onset was driven irreversibly to 556 K. X-ray characterization confirmed the formation of a distorted LaH_{10} based backbone that suggests the formation of ternary or quaternary compounds with substitution at the La and/or H sites. The results provide evidence for hot superconductivity, aligning with recent predictions for higher order hydrides under pressure.

Keywords: superhydrides, superconductivity, high pressure, megabar, higher order lanthanum superhydride
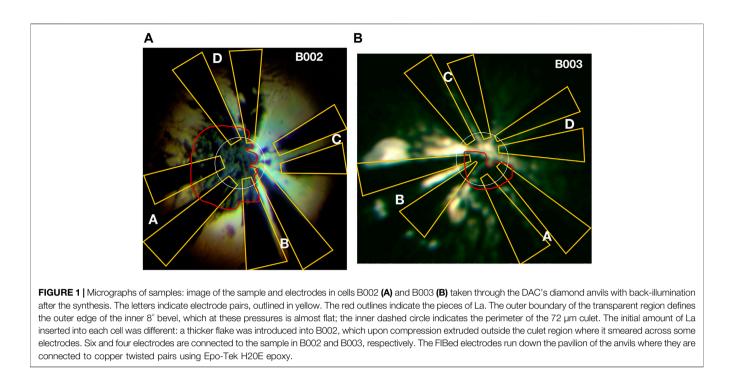
INTRODUCTION

Kamerlingh Onnes' astonishing 1911 discovery of ambient pressure superconductivity in mercury was the serendipitous result of his attempt to validate one of three very different theories that modeled the electrical resistance of metals at low temperature (Onnes, 1911). Since that time, scientists have searched for materials with ever higher transition temperatures driven both by curiosity and technological interests. Initially limited to the elements, the search for superconductivity eventually moved to exploration of binary compounds, which held sway into the 1970's. The approach was very Edisonian in nature and limited by the lack of understanding regarding the mechanism. Phenomenological theories started to be developed about 25 years after the initial discovery of superconductivity. The London equations in 1935 described the Meissner effect (London and London, 1935) and were followed in 1950 with the Ginzburg-Landau thermodynamics theory that portrayed superconductivity as a phase transition with a complex order parameter, the phase of which is constant and describes a macroscopic superconducting quantum state (Ginzburg and Landau, 1950). It was not until 1957 that theory could begin to inform

growth, when Bardeen, Cooper and Schrieffer put forward a microscopic theory of superconductivity (BCS) that invoked phonon interaction to establish electron pairing in a common condensate (Bardeen et al., 1957). The Migdal-Eliashberg theory subsequently provided an extension to the BCS theory (Eliashberg, 1960). For several decades it appeared that superconductivity was fully understood with the maximum critical temperature achieved being 22 K in Nb_3Ge (Gavaler, 1973). Then in 1976, B. Matthias (Matthias et al., 1963) developed a set of rules to assist in the discovery of new superconductors. They included but were not limited to favorable conditions found in high symmetry systems while avoiding magnetic elements, insulators, and oxygen. As growers sought alternate routes to higher transition temperature, the 1970's and 1980's saw the discovery of the heavy fermion systems such as UBe_{13} and $CeCu_2Si_2$ as well as the molecular conductors; however, these materials were quickly overshadowed by the cuprates. At that time, Bednorz and Müller were specifically searching for the next high temperature superconductor in oxides exhibiting a strong Jahn-Teller effect (Bednorz and Müller, 1987). In 1986, as they attempted a growth of a specific Ba-La-Cu-O phase, they discovered within a larger growth a new LBCO phase with a superconducting transition of 35 K. The initial publication (Bednorz and Müller, 1986) that contained only zero field transport measurements and sparce critical current measurements was vigorously contested until several independent groups were able to reproduce the result within a short period of time. This triggered a worldwide race that led to the discovery of YBCO (Wu et al., 1987) with the first T_c above liquid nitrogen temperature.

The history of high pressure research is intimately intertwined with that of superconductivity. At the time when Kamerlingh Onnes and his highly skilled staff were developing novel cryogenic technology, P.W. Bridgman was laying the groundwork for new high pressure techniques. He was awarded the 1946 Nobel Prize in physics for his pioneering work. In the 1950's and 1960's the diamond anvil cell and the gasket (Bassett, 2009) were developed to reach even higher hydrostatic pressures. Their ease of use fostered the rapid growth of the high pressure community. In short order pressure was being used to tune or trigger the superconducting state. The highest T_c observed to date are found in materials under high pressure. For example, the record T_c of 166 K at 23 GPa was held for a couple of decades by the fluorinated cuprate Hg1223 (Monteverdea et al., 2004). In parallel efforts, many of the elements were subjected to pressure. Ca reached a T_c of 29 K when subjected to 216 GPa, the highest for any of the 55 superconducting elements (Sakata et al., 2011). Atomic hydrogen, predicted by Wigner and Huntington (Wigner and Huntington, 1935) in 1935 to be metallic at high pressures, holds great promise as a candidate for room temperature superconductivity and has driven the development of many megabar techniques. Ashcroft (1968) proposed in 1968 that atomic metallic hydrogen at sufficiently high density could be a very high T_c BCS superconductor. In view of the technical challenges to achieve the necessary pressures, Carlsson and Ashcroft (1983) later suggested alternative routes to effectively

produce superconducting atomic hydrogen, including the incorporation of other elements (Eremets et al., 2003). Ashcroft (2004) later extended and recast the above considerations in terms of "chemical pre-compression," a proposal in which H_2 molecules in dense structures might be expected to dissociate at pressures well below those required for pure hydrogen. Advances in crystal structure prediction methods then began to provide experimentalists specific hydrogen-rich targets for higher T_c BCS superconductors (Wang and Ma, 2014; Zurek and Grochala, 2015; Needs and Pickard, 2016; Zhang et al., 2017; Oganov et al., 2019; Semenok et al., 2020) while at the same time theoretical studies focused on understanding the superconducting mechanism (Tanaka et al., 2017; Heil et al., 2019; Liu et al., 2019; Quan et al., 2019; Wang et al., 2019; Errea et al., 2020; Flores-Livas et al., 2020). Notably, this effort led to the prediction (Duan et al., 2014; Li et al., 2014) and, independently, to the experimental discovery (Drozdov et al., 2014; Drozdov et al., 2015) of superconductivity in the H_3S system with a T_c of 203 K, including an isotope study that pointed to BCS behavior. Subsequent simulations of binary structures (Liu et al., 2017; Peng et al., 2017) have now guided the discovery of new hydrides with T_c approaching room temperature. The highest, LaH_{10}, has a critical temperature of 250–260 K and can be pushed to 282 K with thermal cycling that increases the pressure (Drozdov et al., 2019; Hemley et al., 2019; Somayazulu et al., 2019). Somewhat lower values of 227–262 K are reported for related YH_6/YH_9 phases (Troyan et al., 2021; Kong et al., 2021; Snider et al., 2020b). Within the hydrides, only the superconducting transitions in H_3S (Drozdov et al., 2015; Huang et al., 2019), YH_6 (Kong et al., 2021; Snider et al., 2020a; Troyan et al., 2021) and LaH_{10} (Drozdov et al., 2019; Hemley et al., 2019; Somayazulu et al., 2019; Hong et al., 2020) have been experimentally reproduced by independent groups.

With the recent discovery of a 288 K ternary carbonaceous sulfur hydride superconductor (Snider et al., 2020a), what had once been proposed as a goal in and of itself, superconductivity at room temperature now appears to be the stepping off point for still higher transition temperatures. The structure and composition of several possible candidates for this system were determined by Bykova et al. (2021) and there is a possibility that this hydride is a product of C-doping of H_3S (Ge et al., 2020). Much like when the observation of superconductivity in cuprates led to a flurry of discoveries and engineering applications that pushed the critical temperatures in these materials from 40 to 166 K over the course of only a decade (Bednorz and Müller, 1986; Monteverdea et al., 2004), hydrogen-based materials also hold great promise. Early calculations predict that crystalline atomic metallic hydrogen (Ashcroft, 1968; Schneider and Stoll, 1971) has a T_c near room temperature at 500 GPa, which increases to 420 K above 3 TPa (McMahon et al., 2012). Other calculations predict that hydrogen could be a superconducting superfluid under comparable conditions (Babaev et al., 2004). With one study of binary hydrides indicating a maximum T_c in the vicinity of room temperatures at megabar pressures (Flores-Livas et al., 2020), there is now a focus on the possibility of higher critical temperatures in more chemically complex hydride systems. To this end, recent theoretical studies predict a T_c of

FIGURE 1 | Micrographs of samples: image of the sample and electrodes in cells B002 **(A)** and B003 **(B)** taken through the DAC's diamond anvils with back-illumination after the synthesis. The letters indicate electrode pairs, outlined in yellow. The red outlines indicate the pieces of La. The outer boundary of the transparent region defines the outer edge of the inner 8° bevel, which at these pressures is almost flat; the inner dashed circle indicates the perimeter of the 72 μm culet. The initial amount of La inserted into each cell was different: a thicker flake was introduced into B002, which upon compression extruded outside the culet region where it smeared across some electrodes. Six and four electrodes are connected to the sample in B002 and B003, respectively. The FIBed electrodes run down the pavilion of the anvils where they are connected to copper twisted pairs using Epo-Tek H20E epoxy.

473 K in Li_2MgH_6 near 250 GPa (Sun et al., 2019). Thus, experimental access to the megabar regime opens a new chapter in the history of superconductivity by going through the same steps as the ambient pressure explorations, first by developing binary compounds, and now with the exploration of ternary and higher order materials.

The present work was motivated by a desire to extend the p-T-H phase diagram of previous measurements of the lanthanum-based superhydrides (Drozdov et al., 2019; Hemley et al., 2019; Somayazulu et al., 2019; Hong et al., 2020) to fields approaching 100 T. We also sought to examine lower pressure phases such as LaH_6 which are more experimentally accessible. In addition, we hoped to better understand the discrepancies in the values of T_c found in experiments in which LaH_{10} superhydride was synthesized using ammonia borane (NH_3BH_3) as the hydrogen source (Hemley et al., 2019; Somayazulu et al., 2019; Hong et al., 2020). For this purpose, we developed metallic diamond anvil cells (DAC) designed for superhydride studies in DC magnetic fields that are also small enough to fit into pulsed magnets. Made from the hard, high bulk modulus, highly resistive, and non-magnetic superalloy NiCrAl to provide a mechanically stable DAC and limit the eddy-current heating, these DACs can be used to access temperatures down to 15 K in pulsed fields. The optical openings were sufficient to provide a multi-probe environment, which is crucial in these extreme condition studies that produce unique samples.
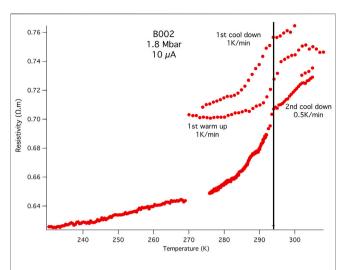
This design was coupled with robust Pt electrodes created by focused ion beam (FIB) techniques to withstand the extreme p-T conditions required to synthesize the superhydrides (Helm et al., 2020). We found that the La-based superhydride initially synthesized by laser-heating at 180 GPa had a reproducible T_c of 294 K. Most remarkably, subjecting the sample to subsequent

thermal cycling shifted the T_c irreversibly to higher temperatures in a fortuitous progression that reached well above 500 K.

RESULTS

We loaded two diamond-anvil cells (DACs) with thin pieces of 99% La and ammonia borane (AB, NH_3BH_3), the hydrogen source and pressure medium (see *Methods* and **Supplementary Information**). Both cells were initially as identical as experimentally possible, with similar FIB-patterned electrodes on each endcap anvil and an MP35N gasket with cBN insert and AB on the piston's anvil. The first cell (B002) was loaded at 180 GPa for LaH_{10} synthesis, whereas the second cell (B003) was loaded at 160 GPa to generate the lower stoichiometry superhydride, LaH_6 (**Figure 1**). After loading, both cells presented electrical shorts between the gasket and the electrodes. Although this contributed to a non-zero resistance, we will show that the electrical circuit is viable for measuring superconducting transitions.

Both La samples were then laser-heated at the HPCAT beamline of the APS. The laser was rastered across the sample at discrete positions to promote the dissociation of AB into cBN and the hydrogen that reacted with the La (**Supplementary Figure S5**). The sample in B002 received about 45 productive laser pulses that coupled to the AB (⌀20 μm laser spot; 4 to 5 pulses at each of nine points on a 10×10 μm grid). The temperature profile of the laser spot falls to room temperature about 30 μm from the center of the spot; therefore, the metal portion of the gasket with an inner diameter of 300 μm is not heated. The synthesis for B003 was stopped prematurely after a few pulses (all at the same position) for fear that a catastrophic failure of the diamond anvils had occurred. This was found not to be the case. Rastering on a grid when using

FIGURE 2 | Initial resistivity measurements: B002 4-probe resistance measurements at different heating and cooling rates using the first electrode configuration **(Supplementary Figure S6)**. The AC current used was 10 µA at 7.5 Hz. There is a transition at 294 K, the upper theoretical limit for the superconducting transition in the binary LaH_{10}. This is also close to the value found experimentally when LaH_{10} is subjected to multiple temperature excursions that increased the pressure and T_c (Hemley et al., 2019; Somayazulu et al., 2019). The two cooling curves at 1 K/min and 0.5 K/min yield the same transition temperature of 294 K, while the 1 K/min warming trace between them shows a transition onset almost 2 K higher.

AB as a hydrogen source and pressure medium necessarily supports a pressure gradient across the sample as compared to liquid hydrogen and is not conducive to a homogeneous growth. This likely explains some of the observed features, especially the multiphase composition, non-zero resistance, and the resistivity background below the transition.

The electrical resistivity was then measured at NHMFL-Tallahassee, using a Quantum Design 16 T PPMS. **Figure 2** shows the first cool down trace from 300 to 230 K for B002 using four of the six available electrodes. A resistance drop is evident at 294 K with no additional transition observed upon cooling to 230 K, the temperature range in which T_c has been previously observed for $LaH_{10\pm\delta}$ systems. As has been observed in other works on LaH_{10} that used AB (Hemley et al., 2019; Somayazulu et al., 2019; Hong et al., 2020), we find a non-zero resistance below the transition and a background below the superconducting transition that can be attributed to hydrogen deficiency during the synthesis (Hong et al., 2020), impurities, grain boundaries, the inhomogeneous nature of the material that makes up the conductive pathway between the voltage taps, and a less than ideal electrical circuit. The latter also played a role in the discovery of superconductivity in S, B, Fe, and oxygen (Struzhkin et al., 1997; Eremets et al., 2001; Shimizu et al., 2001; Shimizu, 2018) at high pressure, where technical challenges forced the use of a quasi-4-probe method that, nonetheless, clearly indicated the presence of a superconducting transition at high pressure.

In an attempt to push above the superconducting state and into the normal state of the B002 sample, we subjected the sample to a series of thermal cycles at 0 T. Perhaps not surprisingly given similar results from other superhydride studies (Drozdov et al., 2014; Drozdov et al.,

2015; Hemley et al., 2019; Somayazulu et al., 2019; Drozdov et al., 2019; Hong et al., 2020; Ahart et al., 2017), these successively higher temperature excursions drove the onset of the transition to higher and higher temperatures. These thermal excursions were temporarily halted at 390 K, is the maximum temperature available in the QD PPMS, to develop an H-T phase diagram for the 360 K material. **Figure 3A** shows the initial and final thermal excursions taken in the PPMS, with the final 0 T onset in T_c appearing near 357 K in this 2-phase superconductor with a combined T_c (90%/10%) width of approximately 5 K. At the base of these transitions we find a small impurity phase. To validate that the electrical circuit in B002 can be used to measure a superconducting sample, B002 and B003 DACs were cooled to 1.9 K. Both exhibit superconducting transitions (**Figure 3B**) attributed to one or more materials—unreacted La (Chen et al., 2020) and PtH (Scheler et al., 2011; Matsuoka et al., 2019). Both DACs have a non-zero resistance to the lowest temperature measured. The resistance of B003 is almost a factor of 10 higher than that of B002, which is most likely due to the difference in thickness of the two samples and the smaller surface area in contact with the electrodes present in B003. When subjected to small applied magnetic fields, these transitions shift according to what would be expected for a conventional superconductor (**Figures 3C,D**).

Four thermal cycles between 370 and 290 K were then performed at 0, 2, 10 and 16 T (**Figure 4A**) to develop an H-T phase diagram. The arrow on the cool down traces indicates the transition onset and is labeled T1. T2 is the approximate transition onset for the warmup curve but is poorly defined due to the evolving nature of the material with warming. Note that the transition in the warming curve for each field is lower in temperature than that found for cooling. Although it is possible that this is due to a lag between the thermometer and the sample, the hysteresis is most likely real as the temperature was swept at 0.2 K/min and the separation is different for each of the four fields. This is opposite to that found in the initial, laser-synthesized material (**Figure 2**).

A clear shift downward with applied field is observed for T2, shifting by 11 K between 0 and 16 T (**Figure 4A**). Assuming that the material is a conventional BCS superconductor, a fit of the data (**Figure 4B**) using the Ginzburg-Landau relation (Ginzburg and Landau, 1950) (Eq. 1):

$$\mu_0 H_c (T) = \mu_0 H_c (0)\left(1 - \left(\frac{T}{T_c}\right)^2\right)$$

Yields a H_c (0 K) of 2.0 (5) kT and 0.4 (1) kT for T1 and T2, respectively. The errors are large for H_c (0 K) as the measurements were performed over a limited field range given the magnitude of T_c. We identified a third transition, T3, which is the temperature at which the hysteresis of the cool down and warmup traces closes. For a type II superconductor, T3 could be interpreted as the melting of the vortex glass and can be fitted by an Almeida-de Thouless equation (Woch et al., 2016) (Eq. 2):

$$H_{irr} = H_{irr} (0\,K)\left(1 - \frac{T}{T_G}\right)^n$$

Where H_{irr} (0 K) is the irreversibility field of this glass transition at 0 K and T_G is the transition temperature at zero field. The fit
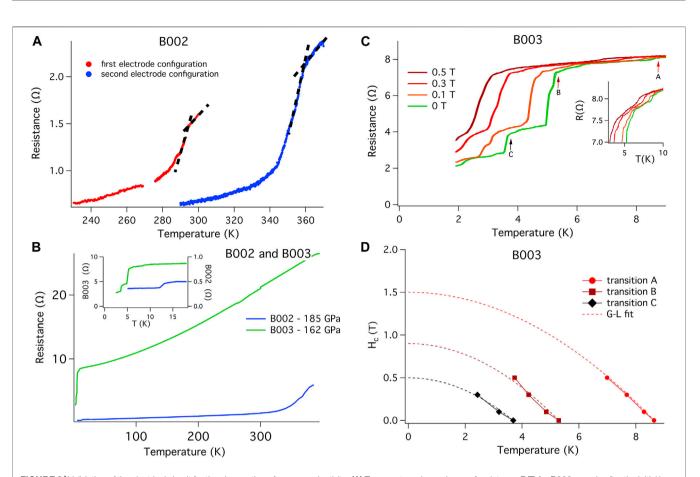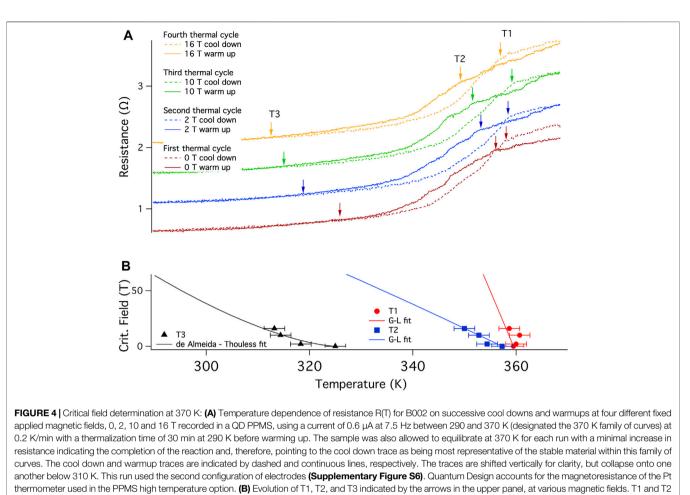
FIGURE 3 | Validation of the electrical circuit for the observation of superconductivity. **(A)** Temperature dependence of resistance R(T) for B002 sample after the initial laser synthesis showing the 294 K temperature transition. The first thermal excursion above 370 K, done with the intent of observing the normal state resistance more fully, transformed the material and yielded a new onset temperature of 357 K. The transition temperature is defined by the intersection of the slopes as indicated by the dotted lines. This second trace was made using a different electrode configuration **(Supplementary Figure S6)**. Temperatures indicated are those of the PPMS chamber. **(B)** R(T) for B002 and B003. The curve of B002 shows the temperature dependence of the background below the 360 K transition. One additional transition is observed below 15 K. The curve of B003 shows no transition between 370 and 10 K, confirming that no high temperature superhydride had been generated. The different R(T) dependencies found in B002 and B003 can be explained in part by the difference in thickness between the two samples, but also because B003 is entirely unreacted La while B002 is strongly dependent on the many factors previously mentioned in the main text. Inset: Low temperature region expanded to more clearly show several transitions that appear below 15 K. Those transitions are attributed to the superconducting transitions of elemental La and PtH_x which are also seen in X-ray patterns for each DAC. To lowest measured temperatures, the resistances of both cells remained non-zero. **(C)** To investigate the superconducting nature of the transitions shown in the insert of **Figure 3B**, we applied various static fields to B003 and measured R(T). Several transitions are observed; the three most prominent ones indicated with arrows, are suppressed with applied field. **(D)** The evolution of the three transitions found in B003 and noted with arrows in **(C)** are shown in an H-T plot; the data is fit using a Ginzburg-Landau formalism. Even though those resistive transitions do not reach a zero resistance state, the Ginzburg-Landau fits make it clear that those resistive transitions are superconducting in nature and validate the electrical circuit, common to both B002 and B003. The non-zero resistance can be attributed to a series resistance pathway composed of the 360 K superconductor, grain boundaries, low temperature superconductors and other impurities. Similar results are found by other groups when using AB as the hydrogen source for superhydride growths. The nature of inhomogeneous growth is evidenced by the X-ray patterns shown in **Supplementary Figure S15** taken in a cut through the sample.

shown uses $n = 1.5$, which is the theoretical value for the exponent for superconductor vortices.

To further investigate the shift in the superconducting transition with field, B002 was then measured in the 41.5 T DC resistive magnet at the NHMFL-Tallahassee. All six working electrodes were used in order to measure two resistance channels simultaneously. We present in the main text only the results from the same configuration as that measured in the PPMS, but the other configuration yielded a similar result (see **Supplementary Figure S7**). Successive thermal cycles carried out to yet higher temperatures in order to establish

the clear signature of the normal state again resulted in a shift of the transition to higher temperatures. The stability of structural and electrically conductive epoxies internal to the DAC and a failed heater limited our measurements to temperatures below 580 K.

Figure 5 shows the cool down traces at 0 T starting from various initial maximum temperatures. The cell remained at each maximum temperature for at least 30 min to allow the synthesis to stabilize as indicated by a steady sample resistance, and was then cooled at 0.5 K/min. With each higher temperature excursion, T_c rises further, eventually reaching a maximum
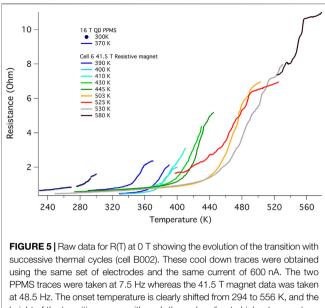
FIGURE 4 | Critical field determination at 370 K: **(A)** Temperature dependence of resistance R(T) for B002 on successive cool downs and warmups at four different fixed applied magnetic fields, 0, 2, 10 and 16 T recorded in a QD PPMS, using a current of 0.6 μA at 7.5 Hz between 290 and 370 K (designated the 370 K family of curves) at 0.2 K/min with a thermalization time of 30 min at 290 K before warming up. The sample was also allowed to equilibrate at 370 K for each run with a minimal increase in resistance indicating the completion of the reaction and, therefore, pointing to the cool down trace as being most representative of the stable material within this family of curves. The cool down and warmup traces are indicated by dashed and continuous lines, respectively. The traces are shifted vertically for clarity, but collapse onto one another below 310 K. This run used the second configuration of electrodes **(Supplementary Figure S6)**. Quantum Design accounts for the magnetoresistance of the Pt thermometer used in the PPMS high temperature option. **(B)** Evolution of T1, T2, and T3 indicated by the arrows in the upper panel, at various magnetic fields. T1 and T2 can be fit using the Ginzburg-Landau theory while data for T3 appears to fit an irreversibility line.

value of 556 K. The amplitude of the transition also increases with each excursion to higher temperatures, which we attribute to an ongoing chemical reaction. Shifts in transition temperature with repeated thermal cycling or laser heating have been documented for several superconducting hydrides (Drozdov et al., 2014; Drozdov et al., 2015; Ahart et al., 2017; Drozdov et al., 2019; Hemley et al., 2019; Somayazulu et al., 2019; Hong et al., 2020). The temperature dependence of the resistance below the transition is almost identical for all the curves, indicating that the various contributions to this background are not affected by this chemical reaction. Due to the evolving nature of the material at high temperatures brought on by these heating cycles, it was not possible to obtain a reliable H-T phase diagram for temperatures higher than 380 K (see **Supplementary Figure S9**).

Synchrotron X-ray diffraction measurements were carried out at the Extreme Conditions Beamline P02.2 at PETRA III (Liermann et al., 2015) in September 2020, 6 months after the laser synthesis that yielded the 294 K superconductor. The availability of a micro-focused, high energy X-ray beam (typically, $2 \times 2 \mu m^2$ focal spot at 42.9 keV or 0.2887 Å) with a large focal length is perfectly suited to interrogate the sample in the special non-magnetic cells used in our studies. The small opening angles (~6° Q) both in the incident and exit directions

and the insulating, low Z gasket (cBN in our case) and small amount of sample pose a challenge in collecting 2D diffraction maps and interpreting them effectively. Two dimensional maps at 3 μm spatial resolution resulted in 2,809 patterns being collected over the 1.5×1.5 mm^2 area depicted in **Supplementary Figure S14**. While we initially set out to examine all the patterns that pointed to the sample between the measuring electrodes **(Supplementary Figure S6)**, we limited ourselves to the sample area at the highest pressures in both cells. Mainly, this was to ensure that we made use of the pressure estimated from diamond Raman which was in turn necessitated due to the fact that even at these high energies, we cannot reliably obtain diffraction from the electrodes which lie outside the transmission window subtended by the exit backing plate. Our discussion is therefore limited to what we can identify on the culet and bridging the relevant electrodes that allowed a four-probe conductivity measurement.

We can easily dispose B003, the cell that was measured to have a pressure of 162 (5) GPa Pressure was measured at the center of the 72 μm culet using the shift in the diamond 1st order Raman line using 532 nm 20 mW excitation. Independently, this was cross calibrated with the Pt diffraction. The difference in pressures so determined was estimated to be of the order +/- 5 GPa and

FIGURE 5 | Raw data for R(T) at 0 T showing the evolution of the transition with successive thermal cycles (cell B002). These cool down traces were obtained using the same set of electrodes and the same current of 600 nA. The two PPMS traces were taken at 7.5 Hz whereas the 41.5 T magnet data was taken at 48.5 Hz. The onset temperature is clearly shifted from 294 to 556 K, and the height of the transition grows with each thermal cycling to higher temperature, opposite to that found for the other superhydrides, and possibly pointing to the ongoing reaction. The cool down for the 556 K was cut short by the failure of the heater. These thermal excursions took place over a period of 1 month **(Supplementary Table S21)** and it would appear that the reaction is not complete **(Supplementary Figure S8)**.

consisting of the sample that did not couple to the heating laser during synthesis. In any laser heating experiment, a common issue is the insufficiency of the thermal buffer (especially at megabar pressures) which in turn impedes proper coupling to the IR laser. In our case, this is compounded by the fact that the thermal buffer is also the hydrogen source and therefore it is not surprising that resistivity measurements indicated a predominance of unreacted La (transition at 5 K). A systematic analysis of the diffraction patterns obtained from the area extending out to the electrodes (**Supplementary Figure S6**) shows only a few diffraction peaks that can be identified as follows (**Figure 6**).

Based on the analysis summarized in **Figure 6**, we can conclude that B003 consists of predominantly unreacted La at pressures below the $R\,\overline{3}\,m$–$Fmmm$ transition identified by Chen et al. (2020). Indeed, this is consistent with the resistivity measurements.

The case of B002 is richer. Resistivity measurements indicate a transition at 294 K that was followed by a monotonic increase in the transition temperature with every cycle of heating and cooling, implying a gradual change in the sample composition. The diffraction measurement is *ex-situ* and made at 300 K after the final thermal cycling presented earlier. A representative diffraction pattern obtained from the culet area is shown in **Figure 7** and summarized in **Table 1** (see **Supplementary Figures S18–S20** for contour plots obtained from diffraction data that highlights the variation in sample composition).

As can be surmised from the residual plotted in **Figure 7**, the diffraction peaks do not have the same widths and the mixture of

phases with different weights (indicative of different overall compositions) can be used to fit the whole pattern. As listed in the table, a total of five phases were identified. The presence of *Fmmm* La and fcc Pt is due to unreacted sample and underlying electrode, and fcc PtH_x is also present. This latter phase and the fcc LaH_{10-x} with smaller peak widths indicate their origin to be due to laser heating and thereby reaction with the hydrogen source in close contact. The presence of rhombohedral LaH_{10-x} is surprising not only due to the complex admixture of this phase with the cubic phase (representative patterns are shown in **Supplementary Figure S17**), but also since these two phases have similar molar volumes. From a standpoint of the molar volume (derived by dividing the observed cell volume by 4 for the fcc phase and 3 for the $R\,\overline{3}\,m$ phase, see **Table 1** and **Figure 8**), we have the following observations: 1) the cubic and rhombohedral phases of LaH_{10-x} have similar unit cell volumes that track close to LaH_8; 2) the volumes of Pt and unreacted (*Fmmm*) La track close to the expected volumes for 175 GPa (this was the pressure estimated from diamond Raman measured before and after synthesis using 532 nm excitation); and 3) while both the phases of LaH_{10-x} show volumes consistent with lower H stoichiometry, the volume of PtH_x (solid black circle in **Figure 8**) shows a stoichiometry consistent with PtH_8 which has not been reported earlier (Semerikova et al., 2020).

These observations allow us to conclude that the apparently lower hydrogen stoichiometry in LaH_{10-x} is not a result of hydrogen deficiency or an incomplete reaction, but rather a result of substitution of H in either/or both fcc and rhombohedral phases by some other ligand (most likely Pt, C, and/or BH_2). While this could be verified by recording the diffraction patterns progressively after each thermal cycle in the resistivity measurements, the current set of observations both in the XRD measurements and the transport measurements indicate these important conclusions: 1) B002, which was successfully laser heated at pressures above 170 GPa, shows a distinctly recognizable backbone fcc LaH_{10-x} structure consistent with the observed resistivity transition above 260 K in the first cooling cycle; 2) successive heating cycles (which progressed to higher temperatures) in B002 resulted in gradual chemical changes to this phase and resulted in a complex admixture of fcc and rhombohedral LaH_{10-x} having similar volumes; and 3) the observed synthesis of PtH_x ($x \sim 8$, hitherto unreported in literature and in any of our earlier laser heating experiments) indicates that such a chemical reaction is due to the availability and proximity of the hydrogen source (unreacted ammonia borane) and this thermal cycling.

Indeed, recent simulations of doped LaH_{10} have predicted such structures leading to higher transition temperatures (Liu et al., 2017; Boeri and Bachelet, 2019; Oganov et al., 2019; Otto, 2019) and this is consistent with the recently reported room temperature superconductivity in the C-S-H system (Snider et al., 2020b) wherein the doping of C in the SH_3 superconductor led to a rise in the transition temperature. While there is no X-ray diffraction data that could be used as a comparison from that particular set of experiments, theoretical simulations (Cui et al., 2020; Sun et al., 2020) indicate that there would be no large
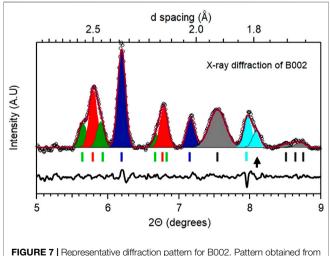
FIGURE 6 | Representative diffraction patterns observed in B003 **(A)**: Patterns obtained from the central culet and surrounding area. The identification of the diffraction peaks is detailed in sub-plot on the **(B)** where the peaks ascribed to La (R $\overline{3}$ m phase) are shaded in grey and the strong Pt (111) diffraction peak is shaded in blue. The expected diffraction peaks from hexagonal $LaH2$ are also indicated by the marker, but there is no evidence of its presence or any of the other lanthanum hydrides below $LaH10$. Not surprisingly, we also notice a broad diffraction peak we ascribe to formation of PtH.

change in lattice symmetry. Recent diffraction data confirms this expectation (Bykova et al., 2021), but no transport measurements were made on the same samples, unlike our measurements reported in this paper.

DISCUSSION

We report the observation of a transition in the resistivity of a La-based superhydride beginning at room temperature that shifts up

FIGURE 7 | Representative diffraction pattern for B002. Pattern obtained from the central culet area of cell B002 at 300 K and 180 GPa. The phases identified in this pattern are listed alongside with the appropriate markers indicating unreacted La (Fmmm, grey), Pt (Fm $\overline{3}$ m, cyan), PtH_x (Fm $\overline{3}$ m, light blue), LaH_{10-x} (R $\overline{3}$ m, green) and LaH_{10-x} (Fm $\overline{3}$ m, red). The arrow points to a diffuse peak that can be attributed to Pt intercalated with H. The estimated cell parameters and cell volumes are listed in **Table 1**.

with thermal excursions to an onset value close to 560 K with a notable concomitant increase in the amplitude.

These high-temperature transitions have the characteristic features of superconductivity, and our X-ray data confirms the presence of both substituted $Fm\overline{3}m$ and $R\overline{3}m$ LaH_{10-x}. However, in the absence of Meissner effect measurements or shifts in the highest T_c with applied magnetic field that are at this time complicated by the ongoing chemical transformations taking place during the measurements, other interpretations must be examined.

First, we address the possibility of a transition from a low-temperature metal to high-temperature semi-metal or insulator. Transitions to insulating states occur with the opening of an energy gap in the Fermi surface, leading to an activated behaviour in resistivity. This is not observed.
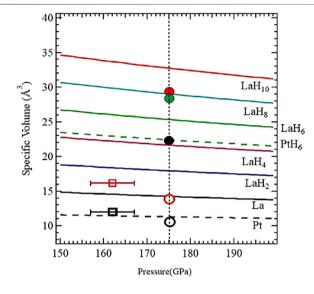
Second, a metal-to-metal phase transition also needs to be ruled out. Such a transition could either arise from a magnetic or a structural phase transition. Magnetic phase transitions would be suppressed or smoothed by an external magnetic field; however, **Supplementary Figure S9** shows rather a sharpening of the onset of the transition at 41 T. In our field sweeps at fixed temperatures below the transition, we see no anomalies.

Third, a high temperature structural phase transition can be ruled out as well. The loading and synthesis done for this work are similar to that used by Somayazulu et al. (2019), the latter which resulted in 260 K superconductor. We performed room temperature X-ray diffraction after the final 600 K excursion. This data, obtained well below the transition temperature in our material, finds both $Fm\overline{3}m$ and $R\overline{3}m$ LaH_{10-x} structures, the former being similar to the room temperature XRD data obtained by Somayazulu in the normal state on their binary LaH_{10} superhydride. Thus, a structural phase transition is improbable.

Finally, one specific aspect that must be addressed is the process of thermal expansion at high pressure. All pressure

TABLE 1 | Cell parameters and volumes for each phase measured.

LaH_{10-x} ($Fm\overline{3}m$, sp. Gr. 225)	a = 4.92 Å, Volume = 29.8 Å^3/mol
LaH_{10-x} ($R\overline{3}m$, Sp. Gr. 166)	a = 3.41 Å, c = 8.76 Å, volume = 29.3 Å^3/mol
Pt ($Fm\overline{3}m$, Sp. Gr. 225)	a = 3.56 Å, volume = 45.1 Å^3, Pressure = 175 ± 5 GPa
PtH ($Fm\overline{3}m$, Sp. Gr. 225)	a = 4.63 Å, volume = 99.1 Å^3
La ($Fmmm$, Sp. Gr. 69)	a = 3.77 Å, b = 3.81 Å, c = 3.85 Å, volume = 13.8 Å^3/atom

FIGURE 8 | The volumes of the assemblage $V_{La} + xV_H$ for various x = 2, 4, 6, 8, and 10 (blue, pink, green, cyan and red) are drawn using the PV relationships of La (Scheler et al., 2011) and H (Loubeyre et al., 2020). We have also plotted the PV curves for La (solid, black) and Pt (dashed, black). The circular symbols (empty and filled) are from B002, and squares are from B003. The solid black circle is PtHx, the solid red and green circles are for LaH_{10-x} $Fm\overline{3}m$ and $R\overline{3}m$ respectively, the open red circle is for La and the open black circle is for Pt.

cells will experience pressure changes as the temperature is varied. These thermal cycles often lead to permanent changes in the pressure due to mechanical relaxation. The pressure of B002 was measured only at room temperature, first in March 2020 after the synthesis at APS; then in July 2020 at ESRF after the thermal excursions that ultimately generated the 556 K transition (**Supplementary Figure S13**). Both measurements showed a maximum pressure at the center of the culet of 178 GPa. Analysis of our subsequent X-ray work confirmed this pressure. We do not know how the pressure varies with temperature in our DACs and no studies have been reported for similar designs. Studies on superconducting systems using controlled pressure changes (with increases substantially greater than thermal expansion effects) have yielded dTc/dp of 1.6 K/GPa for Hg1223 (Gao et al., 1994; Yamamoto et al., 2015), 1 K/GPa for the ternary superhydride C-S-H (Snider et al., 2020b), and a maximum of 8 K/GPa for optimally doped YBCO (Cyr-Choinière et al., 2018). For C-S-H, the initial T_c was about 150 K at 140 GPa,

increasing to 288 K at 271 GPa. Here we observe a 2-fold increase in T_c of 260 K, which is difficult to explain by any mechanical change in the DAC that would allow the pressure to increase an amount sufficient to account for that change and then return to the same room temperature value after many thermal cycles. Most importantly, all the transitions observed were irreversible, and the pressure measured at room temperature during the initial synthesis and 6 months after the thermal cycles were completed remained the same. This argues in favour of a chemical reaction rather than temperature induced pressure changes pushing the transition up in temperature (Please see **Supplementary Information S22** for additional discussions).

Finally, a transition in the metal portion of the gasket rather than sample can be completely ruled out as a similar transition has not been observed in the non-reacted cell B003 and the two DACs have nearly identical circuits and gaskets and are at comparable pressures. The inner diameter of the metal portion is captured between the anvils midway through the second bevel at 300 μm. As noted, at this distance from the location of the laser synthesis that took place on the culet, the temperature rise experienced by the gasket was negligible.

Therefore, we conclude that we have observed a superconducting transition in a metastable superhydride. The initial synthesis used the same ingredients and methods as those used by Somayazulu et al. (2019), and Hong et al. (2020), differing only in the electrodes and nuances introduced by the person loading the cell and carrying out the laser synthesis. The first resistance measurement carried out in the PPMS showed an initial and repeatable transition at 294 K (**Figure 2**) comparable to previous experimental work and the predictions from simulations (Liu et al., 2017; Boeri and Bachelet, 2019; Oganov et al., 2019; Otto, 2019). Resistance measurements were done at various applied fields at 370 K, and the R(T) traces show a shift with field compatible with a Ginzburg-Landau fit, yielding $H_c(0\,K)$ of about 2000 T for the cool down traces (**Figure 4**). This same transition was then tracked in a resistive magnet, shifting irreversibly to higher and higher temperatures *via* successive thermal cycling, the amplitude of the transition growing with each excursion (**Figure 5**). XRD data obtained after the maximum thermal cycle up to 600 K show the formation of a distorted LaH_{10-x} backbone with a volume reduction of about 5% that points to incorporation of one or more elements or ligands that form this higher order hydride.

The non-zero background is not surprising, as it appears in other superhydrides. In our material, we attribute this to the inhomogeneous growth, the short to the gasket, impurities, elemental La and possibly grain boundaries found in the region between the electrodes. This background is seen throughout the thermal cycling and is completely field independent. The XRD patterns in close proximity to the voltage lead tips provides the key to the puzzle, as its shows not only substituted fcc and rhombohedral LaH_{10-x} but also PtH_x and unreacted La and Pt. In both the X-ray and the resistivity data, we could not find any evidence for any binary LaH_x, x < 10. Thus, the portion of the sample showing this very high superconducting transition is electrically in series with these

additional constituents (**Supplementary Figures S15, S17–S20**), which explains the lack of a zero-resistance state. Finally, the field dependance of the transitions below 15 K found in the non-reacted cell B003 show a Ginzburg-Landau behaviour (the multi-phase transitions below 8 K are most likely due to elemental La that is at different pressures since it is smeared out over the culet and the bevels), confirming that our megabar electrical circuit detected superconducting transitions (**Figure 3**), as also demonstrated in the aforementioned literature.

The onset at 294 K is consistent with preliminary observations of T_c above 250 K (Hemley et al., 2019; Somayazulu et al., 2019; Drozdov et al., 2019). The initial T_c of 260 K for LaH_{10} reported in Ref. 39 increases with pressure brought on by thermal cycling to 282 K, close to our starting value of 294 K. The initial increase from 294 to 370 K in our sample may be related to similar behavior observed in the simpler binary hydride H_3Se (Ahart et al., 2017). This has also been described in the preliminary reports of the synthesis of superconducting H_3S (Drozdov et al., 2014). However, this is unlikely, as the maximum predicted transition temperature for the binary $LaH_{10/11}$ system is 288 K (Liu et al., 2017; Peng et al., 2017). Rather, the higher temperature transitions point to additional chemical transformations induced by pressure, shear, and temperature. In addition to B and N from the hydrogen source (NH_3BH_3) or the composite gasket insert (cBN) and the carbon from the epoxy binder, C and Ga from the Pt electrodes also make contact with the La-H and may contribute to the phase assembly of laser heated system with formation of a ternary or higher order system. The thermal excursions performed on the entire cell may have degraded the epoxy binder in the cBN insert, which allowed C and possibly H to diffuse into the sample. Pt, Au from the electrodes, and the amorphous FIBed surface of the diamond may also act as catalysts or catalytic bed, respectively, to help form metastable doped alloys or new stoichiometric compounds. A variety of high p-T induced chemical reactions, phase transformations, or novel phases involving these elements have been documented, even at more modest conditions (Cava et al., 1994; Gregoryanz et al., 2004; Teredesai et al., 2004). Interestingly, the 294 and 360 K cool down traces appear to have only two phases with a third broad phase at the base of these transitions, potentially due to a disordered nature of the latter phase. In contrast, the higher onset temperature transitions have numerous anomalies in the warming traces and fewer in the cooling traces. This supports the idea of a chemical reaction that is activated in temperature, and is possibly incomplete even at 580 K.

The systematic shift of the transition as a result of a temperature treatment deviates from a theoretically predicted superconducting transition of 288 K for the binary La-H system. The background and non-zero resistance can be convincingly traced back to experimental artifacts. Finally, with the exclusion of impurity phases, we consider a picture of a material with a zero resistance at very high temperatures. The XRD data, which is supported by our simulations, clearly support the presence of a substituted LaH_x superhydride superconductor. We do not see any transitions that would be associated with an LaH_x structure close to $x = 8$ as seen in the X-ray and, therefore, we conclude that we have a higher order superhydride with T_c onset of 556 K. Our

observations provide evidence of superconductivity in a metastable compound, perhaps analogous to recent calculations for the Li-Mg-H system in which T_c of 470 K has been predicted within a conventional BCS framework. Recent work on a La-Y hydride ternary (Semenok et al., 2021) and the C-S-H system reported by Snider et al. (2020a) support our discussions and a trend towards room temperature and even higher temperature superconductors.

Additional work is clearly required to characterize the observed fascinating phenomena, including more extensive structural and compositional characterization of the phase (or phases) produced, clarification of p-T-H phase diagrams, and attaining thermodynamic equilibrium. Beyond the surprising observation of "hot" superconductivity, our evidence and discussion presented here emphasize the importance of new multiprobe routes for the creation and characterization of novel materials using multiple extreme environments of pressure, temperature and high magnetic fields.

Note: While in preparation, we have become aware of four publications that attempt to explain our finding (Ge et al., 2021; Guan et al., 2021; Liang et al., 2021; Di Cataldo et al., 2022).

MATERIALS AND METHODS

Diamond Anvil Cells
Our piston-cylinder DACs (Ø9.5 × 39 mm long, **Supplementary Figures S1, S2**, model and photo) are based on concepts presented by Eremets (Eremets, 1996). They were made from hot isostatically pressed (HIPed) NiCrAl [Pascalloy, Tevonics] to reduce vibrations and eddy current heating due to dB/dt which is on the order of 10,000 to 20,000 T/s in pulsed field magnets. 72 μm culet, double bevel (8° × 250 μm, 15° × 350 μm) standard anvils with a 3.75 mm girdle were used.

Focused Ion Beam
For the preparation of robust conductive leads, we used a dual beam FIB system in combination with a scanning electron microscope (SEM). First, a metalorganic gas, trimethyl (methylcylopentadienyl) platinum (IV), is injected into the high-vacuum sample chamber via the nozzle of a gas injection system (GIS) (**Supplementary Figure S3** and **Supplementary Figure S4**). A focused ion stream decomposes the molecules, precisely depositing Pt rich in carbon and gallium (Tao et al., 1990) (typically 30 and 10–20 at%, respectively) onto the anvils. In the same process, the surface of the diamond is amorphized to a depth of approximately 20 nm (for 30 keV gallium ions), allowing the carbon-rich Pt deposit to chemically connect with the broken carbon bonds of the diamond. This chemical bonding results in the mechanical adhesion of FIB-deposits to the diamond, making it extremely robust against mechanical forces. One disadvantage is that the high carbon content reduces the conductivity of such leads significantly (a few Ohms/μm depending on the deposition conditions and the thickness of the layer). In order to realize ohmic lead resistances we deposit, in a second step after a transfer to an external sputter deposition system, a layer (≈100 nm) of pure gold

on top of the prepared platinum ribbons, with Kapton tape used to mask the diamond surface against Au deposition. In the third step, we make use of the high-current gallium beam and etch away excess gold until the amorphous diamond surface is recovered between adjacent taps. The platinum-gold ribbons are then covered with an additional FIB-Pt protection layer ($\approx 1\,\mu m$) running up the pavilion to the culet. Finally, thin FIB-Pt ribbons (with approximately $1\,\mu m$ thickness) are deposited close to the central part of the culet extending the Pt-Au-Pt "sandwich" leads into the sample space, which has a diameter of approximately $40\,\mu m$.

DAC and Sample Assembly

$135\,\mu m$ thick aged MP35N gaskets, located on the piston anvil, were indented to a pressure of 15 GPa using a dummy DAC with the same anvil geometry as B002 and B003 to prevent damage to their electrodes yet provide a gasket which mirrored the anvil shape in these DACs. It was removed and a hole was laser cut (Hrubiak et al., 2015) to a diameter half-way through the second bevel (approximately $300\,\mu m$), polished to remove burrs and most of the extruded region, repositioned on the dummy DAC, and then filled with a dry mixture of cBN powder and epoxy (10% by weight). The gasket was pressed to a load of 25 GPa after which it was laser drilled to a diameter of $40\,\mu m$. This composite gasket was then moved to the piston of the DAC to be used in the experiment. The gasket, secured in a crown affixed to the piston, was brought into a flowing argon filled glove box (O_2 and H_2O content of <1 ppm) and the gasket hole was filled with ammonia borane (NH_3BH_3, or AB) as the hydrogen source and pressure medium. The gasket and gasket crown on the piston are electrically isolated from the rest of the DAC. Pressure measurements required for these various steps in the gasket fabrication were performed at room temperature using the Raman edge of stressed diamond (Akahama and Kawamura, 2006). A third DAC is used to mechanically thin and shear a piece of 99% La (Goodfellow Metals) to expose clean metal. A schmear of the metal, approximately 2-3 μm thick, is extracted from this film and placed on a plastic transfer piston, after which it is brought into the glovebox and pushed against the anvil with FIBed electrodes to form a cold weld. The same plastic transfer anvil is used to initially align this anvil during the assembly of the DAC and the visible impression that remains of that anvil's culet helps ensure that the La is positioned over the electrodes in this second step. To prevent the reaction between La and air, we loaded the sample and sealed the DAC within 30 min of extracting the samples from the freshly exposed metal.

Synthesis

The assembled DAC was then taken to the desired pressure for synthesis using the Raman edge of the stressed diamond. Laser synthesis was performed at HPCAT, Sector 16 of the Advanced Photon Source (APS). The sample heating was single-sided using a IPG YLR-100-1064-WC fiber laser operating in modulation mode (square single pulse) with a total power of 100 W. Temperature measurements were obtained from a $4\,\mu m$ diameter area in the center of the heating spot using an Acton SpectroPro SP2560 imaging spectrograph equipped with a back-illuminated CCD detector (PI-MAX, Princeton Instruments). The laser focal size was $20\,\mu m^2$ and the modulation pulse width was 30 ms (Meng et al., 2015). Heating from the laser spot is negligible beyond $30\,\mu m$ from the spot center. The pressures were measured after the synthesis in March 2020, and for B002, in July 2020 at ESRF after the maximal thermal cycling (see **Supplementary Figure S13**). Additional information on sample synthesis and laser heating methods are described in the supplemental information.

Resistivity Measurements

AC electrical transport measurements in the PPMS were carried out using the internal electronics (7.5 Hz) while measurements in the 41.5 T resistive magnet used two Stanford Research Systems SR860 lockin amplifiers in combination with an SRS CS580 voltage controlled current source to drive a 600 nA current at 48.5 Hz. High magnetic field studies in the 41.5 T resistive magnet at NHMFL-Tallahassee were carried out at fixed fields using consistent sweep rates of 0.5 to 3 K/min in various temperature regions. A custom Janis cryostat with variable temperature insert provided the sample environment. The sample was run under vacuum with a helium partial pressure of 10^{-6} mbar. A small bobbin with three 50 Ohm wire wound heaters in intimate contact with the DAC was mummified in two layers of $12\,\mu m$ copper foil and 37 layers of superinsulation. A Lakeshore Cryotronics Pt-103 thermometer located within the body of the cell and in intimate mechanical contact with the spring and piston was used for both control and sensing. The maximum allowable temperatures of the measurements were limited as the epoxy used to form electrical connection between the twisted pairs and the FIBed electrodes, EPO-TEK H20E, which has a maximum operating temperature of 573 K, began to degrade. The epoxy used to fix the twisted pairs in the DAC, Stycast 2850 FT with catalyst 24 LV, has a maximum operating temperature of 390 K and was completely calcinated after the series of high temperature measurements.

DATA AVAILABILITY STATEMENT

The original contributions presented in the study are included in the article/**Supplementary Material**, further inquiries can be directed to the corresponding authors.

AUTHOR CONTRIBUTIONS

ST and AG conceived, developed, performed the experiments, analyzed the data and wrote the manuscript with exception of the X-ray analysis and narrative which were carried out and written by MS. Sample preparation was performed by ST, AG and MA. MA and RK provided laser synthesis instruction to AG. MS analyzed the X-ray data that was taken by AG and KG. GG performed pressure calibrations across the culets, verifying the integrity of the DACs at the 6-month mark; YM provided beamline user support. TH developed and carried out the FIB process that generated the electrodes. WC assisted with the experiment and performed one method used to correct for the temperature sensor

magnetoresistance. ST, MO and VW designed and fabricated the DACs and supporting equipment. All authors contributed to the discussions and editing of the manuscript.

FUNDING

ACKNOWLEDGMENTS

SUPPLEMENTARY MATERIAL

The Supplementary Material for this article can be found online at: https://www.frontiersin.org/articles/10.3389/femat.2022.837651/full#supplementary-material

REFERENCES

Ahart, M., Mishra, A. K., Somayazulu, M., Park, C. Y., Meng, Y., and Hemley, R. J. (2017). New Hydrides in the S-Se-P-H System Synthesized at High Pressure - High Temperature Conditions. *Bull. Am. Phys. Soc.* Available at: http://meetings.aps.org/link/BAPS.2017.MAR.B35.1.

Akahama, Y., and Kawamura, H. (2006). Pressure Calibration of Diamond Anvil Raman Gauge to 310 GPa. *J. Appl. Phys.* 100, 043516. doi:10.1063/1.2335683

Ashcroft, N. W. (2004). Hydrogen Dominant Metallic Alloys: High Temperature Superconductors? *Phys. Rev. Lett.* 92, 187002. doi:10.1103/physrevlett.92.187002

Ashcroft, N. W. (1968). Metallic Hydrogen: A High-Temperature Superconductor? *Phys. Rev. Lett.* 21, 1748–1749. doi:10.1103/physrevlett.21.1748

Babaev, E., Sudbø, A., and Ashcroft, N. W. (2004). A Superconductor to Superfluid Phase Transition in Liquid Metallic Hydrogen. *Nature* 431, 666–668. doi:10.1038/nature02910

Bardeen, J., Cooper, L. N., and Schrieffer, J. R. (1957). Theory of Superconductivity. *Phys. Rev.* 108, 1175–1204. doi:10.1103/physrev.108.1175

Bassett, W. A. (2009). Diamond Anvil Cell, 50th Birthday. *High Press. Res.* 29, 163–186. doi:10.1080/08957950802597239

Bednorz, J. G., and Müller, K. A. (1986). Possible high T_c Superconductivity in the Ba-La-Cu-O System. *Z. Physik B - Condensed Matter* 64, 189–193. doi:10.1007/bf01303701

Bednorz, J. G., and Müller, K. A. (1987). Perovskite-type Oxides – the New Approach to High-T_c Superconductivity. *Rev. Mod. Phys.* 60, 585. doi:10.1103/RevModPhys.60.585

Boeri, L., and Bachelet, G. B. (2019), The Road to Room-Temperature Conventional Superconductivity. *J.Phys. Condens. Matter* 31, 234002. doi:10.1088/1361-648X/ab0db2

Bykova, E., Bykov, M., Chariton, S., Prakapenka, V. B., Glazyrin, K., Aslandukov, A., et al. (2021). Structure and Composition of C-S-H Compounds up to 143 GPa. *Phys. Rev. B* 103, L140105. doi:10.1103/physrevb.103.l140105

Carlsson, A. E., and Ashcroft, N. W. (1983). Approaches for Reducing the Insulator-Metal Transition Pressure in Hydrogen. *Phys. Rev. Lett.* 50, 1305–1308. doi:10.1103/physrevlett.50.1305

Cava, R. J., Zandbergen, H. W., Batlogg, B., Eisaki, H., Takagi, H., Krajewski, J. J., et al. (1994). Superconductivity in Lanthanum Nickel Boro-Nitride. *Nature* 372, 245–247. doi:10.1038/372245a0

Chen, W., Semenok, D. V., Troyan, I. A., Ivanova, A. G., Huang, X., Oganov, A. R., et al. (2020). Superconductivity and Equation of State of Lanthanum at Megabar Pressures. *Phys. Rev. B* 102, 134510. doi:10.1103/physrevb.102.134510

Cui, W., Bi, T., ShiLi, J. Y., Li, Y., Liu, H., Zurek, E., et al. (2020). Route to High-T_c Superconductivity via CH_4-intercalated H_3S Hydride Perovskites. *Phys. Rev. B* 101, 134504. doi:10.1103/physrevb.101.134504

Cyr-Choinière, O., LeBoeuf, D., Badoux, S., Dufour-Beauséjour, S., Bonn, D. A., Hardy, W. N., et al. (2018). Sensitivity of Tc to Pressure and Magnetic Field in the Cuprate Superconductor $YBa_2Cu_3O_y$: Evidence of Charge-Order Suppression by Pressure. *Phys. Rev. B* 98, 064513. doi:10.1103/physrevb.98.064513

Di Cataldo, S., von der Linden, W., and Boeri, L. (2022). First-principles Search of Hot Superconductivity in La-X-H Ternary Hydrides. *Npj Comput. Mater.* 8, 2. doi:10.1038/s41524-021-00691-6

Drozdov, A. P., Eremets, M. I., and Troyan, I. A., Conventional Superconductivity at 190 K at High Pressures. arXiv1412.0460v1 (2014).

Drozdov, A. P., Eremets, M. I., Troyan, I. A., Ksenofontov, V., and Shylin, S. I. (2015). Conventional Superconductivity at 203 Kelvin at High Pressures in the Sulfur Hydride System. *Nature* 525, 73–76. doi:10.1038/nature14964

Drozdov, A. P., Kong, P. P., Minkov, V. S., Besedin, S. P., Kuzovnikov, M. A., Mozaffari, S., et al. (2019). Superconductivity at 250 K in Lanthanum Hydride under High Pressures. *Nature* 569, 528–531. doi:10.1038/s41586-019-1201-8

Duan, D., Liu, Y., Tian, F., Li, D., Huang, X., Zhao, Z., et al. (2014). Pressure-induced Metallization of Dense $(H_2S)_2H_2$ with High-T_c Superconductivity. *Sci. Rep.* 4, 6968. doi:10.1038/srep06968

Eliashberg, G. M. (1960). Interactions between Electrons and Lattice Vibrations in a Superconductor. *Zh. Eksperim. I Teor. Fiz. Soviet Phys. JETP* 3811, 966696–966702.

Eremets, M. I. (1996). *High Pressure Experimental Methods*. Oxford University Press.

Eremets, M. I., Struzhkin, V. V., Mao, H. -K., and Hemley, R. J. (2001). Superconductivity in Boron. *Science* 293, 272–274. doi:10.1126/science.1062286

Eremets, M., Struzhkin, V. V., Mao, H. -K., and Hemley, R. J. (2003). Exploring Superconductivity in Low-Z Materials at Megabar Pressures. *Physica B: Condensed Matter* 329-333, 1312–1316. doi:10.1016/s0921-4526(02)02138-5

Errea, I., Belli, F., Monacelli, L., Sanna, A., Koretsune, T., Tadano, T., et al. (2020). Quantum crystal Structure in the 250-kelvin Superconducting Lanthanum Hydride. *Nature* 578, 66–69. doi:10.1038/s41586-020-1955-z

Fei, Y., Mao, H. -K., and Hemley, R. J. (1993). Thermal Expansivity, Bulk Modulus, and Melting Curve of H2O-Ice VII to 20 GPa. *J. Chem. Phys.* 99, 5369–5373. doi:10.1063/1.465980

Flores-Livas, J. A., Boeri, L., Sanna, A., Profeta, G., Arita, R., and Eremets, M. (2020). A Perspective on Conventional High-Temperature Superconductors at High Pressure: Methods and Materials. *Phys. Rep.* 856, 1–78. doi:10.1016/j.physrep.2020.02.003

Gao, L., Xue, Y. Y., Chen, F., Xiong, Q., Meng, R. L., Ramirez, D., et al. (1994). Superconductivity up to 164 K inHgBa2Cam−1CumO2m+2+δ(m=1, 2, and 3) under Quasihydrostatic Pressures. *Phys. Rev. B* 50, 4260–4263. doi:10.1103/physrevb.50.4260

Garai, J., Chen, J., and Telekes, G. (2011). P-V-T Equation of State of Epsilon Iron and its Densities at Core Conditions. *Am. Mineral.* 96 (5–6), 828–832. doi:10.2138/am.2011.3612

Gavaler, J. R. (1973). Superconductivity in Nb-Ge Films above 22 K. *Appl. Phys. Lett.* 23, 480–482. doi:10.1063/1.1654966

Ge, Y., Zhang, F., Dias, R. P., Hemley, R. J., and Yao, Y. (2020). Hole-doped Room-Temperature Superconductivity in H3S1-xZ (Z=C, Si). *Mater. Today Phys.* 15, 100330. doi:10.1016/j.mtphys.2020.100330

Ge, Y., Zhang, F., and Hemley, R. J. (2021). Room-temperature Superconductivity in boron- and Nitrogen-Doped Lanthanum Superhydride. *Phys. Rev. B* 104, 214505. doi:10.1103/physrevb.104.214505

Geballe, Z. M., Liu, H., Mishra, A. K., Ahart, M., Somayazulu, M., Meng, Y., et al. (2018). Synthesis and Stability of Lanthanum Superhydrides. *Angew. Chem. Int. Ed.* 57, 688–692. doi:10.1002/anie.201709970

Ginzburg, V. L., and Landau, L. D. (1950). On the Theory of Superconductivity. *Zh. Eksp. Teor. Fiz.* 20, 1064–1082.

Graf, D. E., Stillwell, R. L., Purcell, K. M., and Tozer, S. W. (2011). Nonmetallic Gasket and Miniature Plastic Turnbuckle Diamond Anvil Cell for Pulsed Magnetic Field Studies at Cryogenic Temperatures. *High Press. Res.* 4 (31), 533–543. doi:10.1080/08957959.2011.633909

Gregoryanz, E., Sanloup, C., Somayazulu, M., Badro, J., Fiquet, G., Mao, H. -K., et al. (2004). Synthesis and Characterization of a Binary noble Metal Nitride. *Nat. Mater* 3, 294–297. doi:10.1038/nmat1115

Guan, P.-W., Hemley, R. J., and Viswanathan, V. (2021). Combining Pressure and Electrochemistry to Synthesize Superhydrides. *Proc. Natl. Acad. Sci. USA* 118 (46), e2110470118. doi:10.1073/pnas.2110470118

Heil, C., di Cataldo, S., Bachelet, G. B., and Boeri, L. (2019). Superconductivity in Sodalite-like Yttrium Hydride Clathrates. *Phys. Rev. B* 99 (R), 220502. doi:10.1103/physrevb.99.220502

Helm, T., Grockowiak, A. D., Balakirev, F. F., Singleton, J., Betts, J. B., Shirer, K. R., et al. (2020). Non-monotonic Pressure Dependence of High-Field Nematicity and Magnetism in CeRhIn5. *Nat. Commun.* 11, 3482. doi:10.1038/s41467-020-17274-6

Hemley, R. J., Ahart, M., Liu, H., and Somayazulu, M. (2019). "Road to Room-Temperature Superconductivity: Tc above 260 K in Lanthanum Superhydride under Pressure,". Editor M. A. Alario y Franco, 199–213. Proc. Ram on Areces Symp. Superconductivity and Pressure: A Fruitful Relationship on the Road to Room Temperature Superconductivity, Madrid, Spain, May 21–22, 2018.

Hong, F., Yang, L., Shan, P., Yang, P., Liu, Z., Sun, J., et al. (2020). Superconductivity of Lanthanum Superhydride Investigated Using the Standard Four-Probe Configuration under High Pressures. *Chin. Phys. Lett.* 37, 107401. doi:10.1088/0256-307x/37/10/107401

Howard, J. (2018). Fastai. Avalableat: https://github.com/fastai/fastai.

Hrubiak, R., Sinogeikin, S., Rod, E., and Shen, G. (2015). The Laser Micro-machining System for Diamond Anvil Cell Experiments and General Precision Machining Applications at the High Pressure Collaborative Access Team. *Rev. Sci. Instrum.* 86, 072202. doi:10.1063/1.4926889

Huang, X., Wang, X., Duan, D., Sundqvist, B., Li, X., Huang, Y., et al. (2019). High-temperature Superconductivity in Sulfur Hydride Evidenced by Alternating-Current Magnetic Susceptibility. *Natl. Sci. Rev.* 6, 713–718. doi:10.1093/nsr/nwz061

Kong, P., Minkov, V. S., Kuzovnikov, M. A., Besedin, L., Balicas, L., Drozdov, A., et al. (2021) Superconductivity up to 243 K in Yttrium Hydrides under High Pressure. *Nat. Commun.* 12, 5075. doi:10.1038/s41467-021-25372-2

Li, Y., Hao, J., Liu, H., Li, Y., and Ma, Y. (2014). The Metallization and Superconductivity of Dense Hydrogen Sulfide. *J. Chem. Phys.* 140, 174712. doi:10.1063/1.4874158

Liang, X., Bergara, A., Wei, X., Song, X., Wang, L., Sun, R., et al. (2021). Prediction of High-Tc Superconductivity in Ternary Lanthanum Borohydrides. *Phys. Rev. B* 104, 134501. doi:10.1103/physrevb.104.134501

Liermann, H.-P., Konôpková, Z., Morgenroth, W., Glazyrin, K., Bednarčik, J., McBride, E. E., et al. (2015). The Extreme Conditions Beamline P02.2 and the Extreme Conditions Science Infrastructure at PETRA III. *J. Synchrotron Radiat.* 22, 908–924. doi:10.1107/s1600577515005937

Liu, H., Naumov, I. I., Hoffmann, R., Ashcroft, N. W., and Hemley, R. J. (2017). Potential High-Superconducting Lanthanum and Yttrium Hydrides at High Pressure. *Proc. Natl. Acad. Sci.* 114, 6990–6995.

Liu, L., Wang, C., Yi, S., Kim, K. W., Kim, J., and Cho, J.-H. (2019). Microscopic Mechanism of Room-Temperature Superconductivity in Compressed LaH10. *Phys. Rev. B* 99, 140501. doi:10.1103/physrevb.99.140501

London, F., and London, H. (1935). The Electromagnetic Equations of the Supraconductor. *Proc. R. Soc. Lond. A.* 149, 71–88.

Loubeyre, P., Occelli, F., and Dumas, P. (2020). Synchrotron Infrared Spectroscopic Evidence of the Probable Transition to Metal Hydrogen. *Nature* 577, 631–635. doi:10.1038/s41586-019-1927-3

Matsuoka, T., Hishida, M., Kuno, K., Hirao, N., Ohishi, Y., Sasaki, S., et al. (2019). Superconductivity of Platinum Hydride. *Phys. Rev. B* 99, 144511.

Matthias, B. T., Geballe, T. H., and Compton, V. B. (1963). Superconductivity. *Rev. Mod. Phys.* 35, 1–22. doi:10.1103/revmodphys.35.1

McMahon, J. M., Morales, M. A., Pierleoni, C., and Ceperley, D. M. (2012). The Properties of Hydrogen and Helium under Extreme Conditions. *Rev. Mod. Phys.* 84, 1607–1653. doi:10.1103/revmodphys.84.1607

Meng, Y., Hrubiak, R., Rod, E., Boehler, R., and Shen, G. (2015). New Developments in Laser-Heated Diamond Anvil Cell with *In Situ* Synchrotron X-ray Diffraction at High Pressure Collaborative Access Team. *Rev. Sci. Instrum.* 86, 072201. doi:10.1063/1.4926895

Monteverdea, M., Nunez-Regueiro, M., Acha, C., Lokshin, K. A., Pavlov, D. A., Putilin, S. N., et al. (2004). Fluorinated Hg-1223 under Pressure: the Ultimate Tc of the Cuprates? *Physica C* 23, 408–410.

Needs, R. J., and Pickard, C. J. (2016). Perspective: Role of Structure Prediction in Materials Discovery and Design. *APL Mater.* 4, 053210. doi:10.1063/1.4949361

Oganov, A. R., Pickard, C. J., Zhu, Q., and Needs, R. J. (2019). Structure Prediction Drives Materials Discovery. *Nat. Rev. Mater.* 4, 331–348. doi:10.1038/s41578-019-0101-8

Onnes, H. K. (1911). The Disappearance of the Resistivity of Mercury. *Comm. Leiden* 122, 2.

Otto, H. H. (2019). Super-Hydrides of Lanthanum and Yttrium: On Optimal Conditions for Achieving Near Room Temperature Superconductivity. *Wjcmp* 09, 22–36. doi:10.4236/wjcmp.2019.91002

Paszke, A., Gross, S., Massa, F., Lever, A., Chanan, G., Killen, T., et al. (2019). Pytorch: An Imperative Style, High-Performance Deep Learning Library. *Adv. Neural Inf. Process. Syst.* 32, 8024–8035.

Peng, F., Sun, Y., Pickard, C. J., Needs, R. J., Wu, Q., and Ma, Y. (2017). Hydrogen Clathrate Structures in Rare Earth Hydrides at High Pressures: Possible Route to Room-Temperature Superconductivity. *Phys. Rev. Lett.* 119, 107001. doi:10.1103/physrevlett.119.107001

Quan, Y., Ghosh, S. S., and Pickett, W. E. (2019). Compressed Hydrides as Metallic Hydrogen Superconductors. *Phys. Rev. B* 100, 184505. doi:10.1103/physrevb.100.184505

Sakata, M., Nakamoto, Y., Shimizu, K., Matsuoka, T., and Ohishi, Y. (2011). Superconducting State of Ca-VII below a Critical Temperature of 29 K at a Pressure of 216 GPa. *Phys. Rev. B* 83 (R), 220512. doi:10.1103/physrevb.83.220512

Scheler, T., Degtyareva, O., Marqués, M., Guillaume, C. L., Proctor, J. E., Evans, S., et al. (2011). Synthesis and Properties of Platinum Hydride. *Phys. Rev. B* 83, 214106. doi:10.1103/physrevb.83.214106

Schneider, T., and Stoll, E. (1971). Metallic Hydrogen II High-Temperature Superconductivity. *Physica* 55, 702–710. doi:10.1016/0031-8914(71)90322-3

Semenok, D. V., Kruglov, I. A., Savkin, I. A., Kvashnin, A. G., and Oganov, A. R. (2020). On Distribution of Superconductivity in Metal Hydrides. *Curr. Opin. Solid State. Mater. Sci.* 24, 100808. doi:10.1016/j.cossms.2020.100808

Semenok, D. V., Troyan, I., Ivanova, A. G., Kvashnin, A. G., Kruglov, I. A., Hanfland, M., et al. (2021) Superconductivity at 253 K in Lanthanum-Yttrium Ternary Hydrides. *Matls. Today* 48, 18–28. doi:10.1016/j.mattod.2021.03.025

Semerikova, A., Chanyshen, D., Glazyrin, K., Pakhomova, A., Kurnosov, A., Litasov, K., et al. (2020). Face-Centered Cubic Platinum Hydride and Phase Diagram of PtH. *Eur. J. Inorg. Chem.*, 4532–4538. doi:10.1002/ejic.202000849

Shimizu, K., Kimura, T., Furomoto, S., Takeda, K., Kontani, K., Onuki, Y., et al. (2001). Superconductivity in the Non-magnetic State of Iron under Pressure. *Nature* 412, 316–318. doi:10.1038/35085536

Shimizu, K. (2018). Superconducting Elements under High Pressure. *Physica C: Superconductivity its Appl.* 552, 30–33. doi:10.1016/j.physc.2018.05.012

Snider, E., Dasenbrock-Gammon, N., McBride, R., Debessai, M., Vindana, H., Vencatasamy, K., et al. (2020a). Room-temperature Superconductivity in a Carbonaceous Sulfur Hydride. *Nature* 586, 373–377. doi:10.1038/s41586-020-2801-z

Snider, E., Gammon, N., Mcbride, R., Wang, X., Meyers, N., Zurek, E., et al. (2020b). Superconductivity to 262 Kelvin via Catalyzed Hydrogenation of Yttrium at High Pressures. *Phys. Rev. Lett.* 126, 117003.

Somayazulu, M., Ahart, M., Mishra, A. K., Geballe, Z. M., Baldini, M., Meng, Y., et al. (2019). Evidence for Superconductivity above 260 K in Lanthanum Superhydride at Megabar Pressures. *Phys. Rev. Lett.* 122, 027001. doi:10.1103/PhysRevLett.122.027001

Struzhkin, V. V., Hemley, R. J., Mao, H. -K., and Timofeev, Y. A. (1997). Superconductivity at 10-17 K in Compressed sulphur. *Nature* 390, 382–384. doi:10.1038/37074

Sun, Y., Lv, J., Xie, Y., Liu, H., and Ma, Y. (2019). Route to a Superconducting Phase above Room Temperature in Electron-Doped Hydride Compounds under High Pressure. *Phys. Rev. Lett.* 123, 097001. doi:10.1103/PhysRevLett.123.097001

Sun, Y., Tian, Y., Jiang, B., Li, X., Li, H., Iitaka, T., et al. (2020). Computational Discovery of a Dynamically Stable Cubic SH_3-like High-Temperature Superconductor at 100 GPa via CH_4 Intercalation. *Phys. Rev. B* 101, 174102. doi:10.1103/physrevb.101.174102

Tanaka, K., Tse, J. S., and Liu, H. (2017). Electron-phonon Coupling Mechanisms for Hydrogen-Rich Metals at High Pressure. *Phys. Rev. B* 96. doi:10.1103/physrevb.96.100502

Tao, T., Ro, J., and MeIngailis, J. (1990). Focused Ion Beam Induced Deposition of Platinum. *J. Vac. Sci. Technol. B* 8, 1826. doi:10.1116/1.585167

Teredesai, P., Muthu, D. V. S., Chandrabhas, N., Meenakshi, S., Vijayakumar, V., Modak, P., et al. (2004). High Pressure Phase Transition in Metallic LaB_6: Raman and X-ray Diffraction Studies. *Solid State. Commun.* 129, 791–796. doi:10.1016/j.ssc.2003.12.041

Troyan, I. A., Semenok, D. V., Kvashnin, A. G., Sadakov, A. V., Sobolevskiy, O. A., Pudalov, V. M., et al. (2021). Anomalous High-Temperature Superconductivity in YH_6. *Adv. Mater.* 33, e2006832–9648. doi:10.1002/adma.202006832

Wang, C., Yi, S., and Cho, J.-H. (2019). Pressure Dependence of the Superconducting Transition Temperature of Compressed LaH_{10}. *Phys. Rev. B* 100 (R), 060502. doi:10.1103/physrevb.100.060502

Wang, Y., and Ma, Y. (2014). Perspective: Crystal Structure Prediction at High Pressures. *J. Chem. Phys.* 140, 040901. doi:10.1063/1.4861966

Wigner, E., and Huntington, H. B. (1935). On the Possibility of a Metallic Modification of Hydrogen. *J. Chem. Phys.* 3, 764–770.

Woch, W. M., Chrobak, M., Kowalik, M., Zalecki, R., Przewoźnik, J., and Kapusta, C. (2016). Magnetoresistance and Irreversibility Fields of Bismuth-Based 1G Tape. *J. Supercond Nov Magn.* 29, 2333–2336. doi:10.1007/s10948-016-3536-9

Wu, M. K., Ashburn, J. R., Torng, C. J., Hor, P. H., Meng, R. L., Gao, L., et al. (1987). Superconductivity at 93 K in a New Mixed-phase Y-Ba-Cu-O Compound System at Ambient Pressure. *Phys. Rev. Lett.* 58, 908–910. doi:10.1103/physrevlett.58.908

Yamamoto, A., Takeshita, N., Terakura, C., and Tokura, Y. (2015). High Pressure Effects Revisited for the Cuprate Superconductor Family with Highest Critical Temperature. *Nat. Commun.* 6, 8990. doi:10.1038/ncomms9990

Zhang, L., Wang, Y., Lv, J., and Ma, Y. (2017). Materials Discovery at High Pressures. *Nat. Rev. Mater.* 2, 17005. doi:10.1038/natrevmats.2017.5

Zurek, E., and Grochala, W. (2015). Predicting crystal Structures and Properties of Matter under Extreme Conditions via Quantum Mechanics: the Pressure Is on. *Phys. Chem. Chem. Phys.* 17, 2917–2934. doi:10.1039/c4cp04445b